Available online at www.sciencedirect.com

SciVerse ScienceDirect

Ceramics International 38 (2012) 6651–6658

CERAMICS INTERNATIONAL

www.elsevier.com/locate/ceramint

Electrical and dielectric characteristics of erbium-added $ZnO–V_2O_5$-based varistor ceramics

Choon-Woo Nahm*

Semiconductor Ceramics Laboratory, Department of Electrical Engineering, Dongeui University, Busan 614-714, Republic of Korea

Received 7 March 2012; received in revised form 15 May 2012; accepted 17 May 2012
Available online 23 May 2012

Abstract

This paper focuses on that the erbium-added $ZnO–V_2O_5$-based ceramics are attained at a sintering temperature as low as 875 °C. The effect of Er_2O_3 addition on microstructure, electrical properties, and dielectric characteristics has been investigated. Increasing the amount of Er_2O_3 slightly increased the densities of sintered pellets in the range of 5.52–5.59 g/cm^3. The increase in the amount of Er_2O_3 increased the breakdown field from 6991 to 7408 V/cm up to 0.1 mol%, whereas a further addition decreased it. The sample added with 0.1 mol% Er_2O_3 exhibited the highest nonlinear coefficient ($\alpha=55$) and the sample added with 0.25 mol% Er_2O_3 exhibited the lowest nonlinear coefficient ($\alpha=14$). The donor concentration increased from 2.92×10^{17} to 8.48×10^{17} cm^{-3} with an increase in the amount of Er_2O_3.

Keywords: B. Grain boundaries; C. Dielectric properties; C. Electrical properties; D. ZnO

1. Introduction

Polycrystalline ZnO varistor ceramics are made by sintering ZnO powders mixed with minor additives containing one of primary constituents such as Bi_2O_3 and Pr_6O_{11}, and subordinate constituents such as CoO, MnO_2, Cr_2O_3, etc, Microstructurally, they are composed of semiconducting ZnO grains, which are surrounded by very insulating intergranular layers at grain boundaries. In detail speaking, ZnO ceramics have a distinctive microstructure, which a unit structure consisting of ZnO grain-intergranular layer-ZnO grain is distributed three-dimensionally through overall ceramics. Electrically, they are similar to back-to-back Zener diode in the current–voltage relation. Functionally, they are voltage switching devices, which has a property known as nonlinear resistance. At low applied voltages, the varistor ceramics furnish very high resistance of about $10^{12}\,\Omega$ cm and act essentially like open-circuits. Above a certain threshold voltage known as a protection level, the resistance quite reduces substantially. When a transient experienced, the protection level is exceeded and the varistor resistance drops. This allows current to flow through the varistors to ground rather than the circuits. As a result, they have been extensively used to protect various semiconductor devices, electronic circuits, and electric power systems from dangerous transient voltages [1,2].

ZnO varistor ceramics cannot exhibit a nonlinear electrical behavior without adding heavy elements with large ionic radii such as Bi, Pr, Ba, etc. Commercial $ZnO–Bi_2O_3$ (or Pr_6O_{11})-based chip varistor ceramics cannot be co-sintered with an Ag inner-electrode because of the high sintering temperature beyond 1000 °C [3,4]. Therefore, it is inevitable to use the Pd or Pt as inner-electrodes, which will keep the high manufacturing cost. New $ZnO–V_2O_5$ system is potential chip varistor ceramics, which can use only Ag inner-electrode without using expensive Pd or Pt because this system can be sintered at a relatively low temperature of approximately 900 °C [5].

On the whole, a study on $ZnO–V_2O_5$-based ceramics is in its early stages in many aspects for applications. The $ZnO–V_2O_5$-based ceramics requires specific additives and sintering process in order to have higher nonlinear

*Tel.: +82 51 890 1669; fax: +82 51 890 1664.
E-mail address: cwnahm@deu.ac.kr

0272-8842/$36.00 © 2012 Elsevier Ltd and Techna Group S.r.l. All rights reserved.
http://dx.doi.org/10.1016/j.ceramint.2012.05.052

properties and stability [6–12]. It is very important to understand the influences of additives and sintering process on nonlinear properties [13–16]. No the erbium-added $ZnO–V_2O_5$-based varistor ceramics sintered at temperature below 900 °C have been reported until now. If the ceramics can be sintered at lower temperature, with satisfactory sinterability and nonlinear properties, obviously this will provide some more information about the optimization for ceramic composition and sintering process.

The purpose of this study is to address the microstructure, electrical properties, and dielectric characteristics of the erbium-added $ZnO–V_2O_5$-based ceramics sintered at temperature as low as 875 °C and new remarkable result was obtained compared with literature reported previously [17].

2. Experimental procedure

2.1. Sample preparation

High purity (> 99.9%) reagent-grade raw powders, with less than 1 μm in particle size, were prepared in the proportion of (97.4 − x) mol% ZnO, 0.5 mol% V_2O_5, 2.0 mol% MnO_2, 0.1 mol% Nb_2O_5, and x mol% Er_2O_3 (x = 0.0, 0.05, 0.1, and 0.25). The weighed powders were mixed by ball milling with zirconia balls and acetone in a polypropylene bottle for 24 h. The dried mixture was mixed into a container with acetone and 0.8 wt% polyvinyl butyral (PVB) binder of powder weight. After drying, the mixture was granulated by sieving through a 100-mesh screen to produce starting powder. The powder was pressed into disk-shaped pellet of 10 mm in diameter and 1.5 mm in thickness at a pressure of 100 MPa. The pellets were sintered at 875 °C in air for 3 h and furnace-cooled to room temperature. The heating and cooling rates were 4 °C/min. The final pellets were about 8 mm in diameter and 1.0 mm in thickness. Silver paste was coated on both faces of the pellets and the electrodes were formed by heating it at 550 °C for 10 min. The electrodes were 5 mm in diameter. Finally, after the lead wire is soldered to both electrodes, the samples were packaged by dipping it into a thermoplastic resin powder.

2.2. Microstructure characterization

The sintered pellets was lapped with SiC paper and polished with Al_2O_3 powders. The polished pellets were chemically etched with $1HClO_4$:$1000H_2O$ for 25 s at 25 °C. The surface microstructure of the samples was examined by a

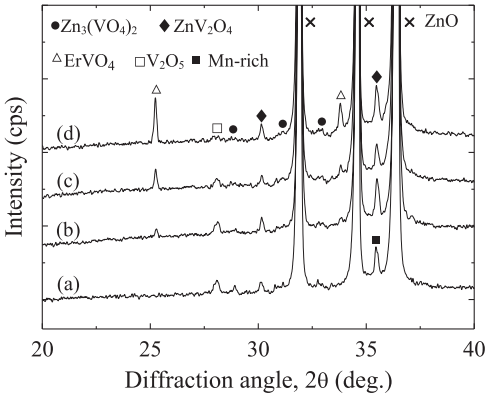

Fig. 2. XRD patterns of the samples with different amounts of Er_2O_3: (a) 0.0 mol%, (b) 0.05 mol%, (c) 0.1 mol%, and (d) 0.25 mol%.

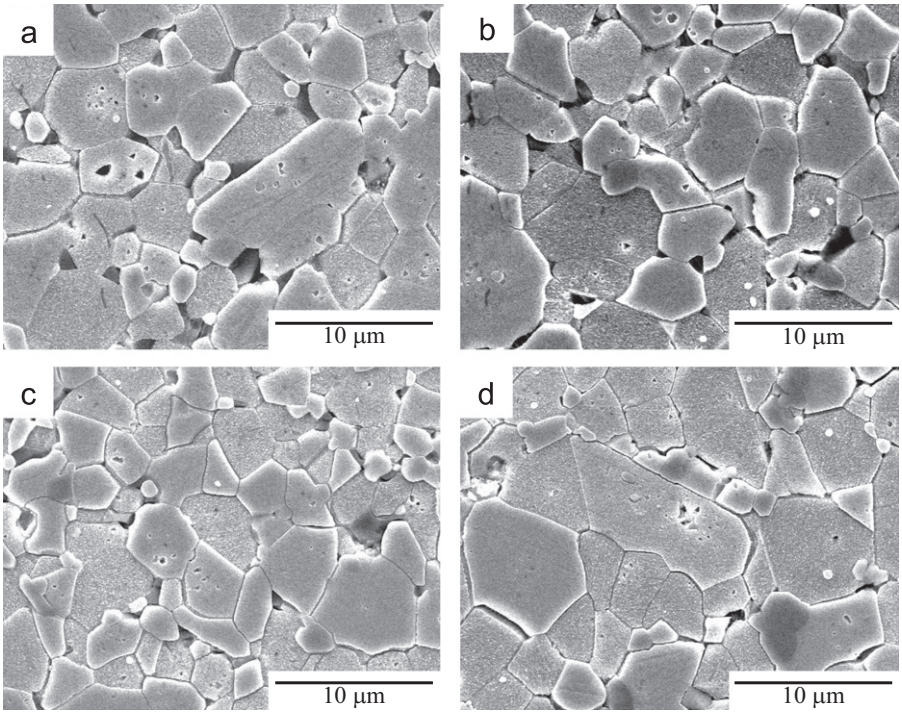

Fig. 1. SEM micrographs of the samples with different amounts of Er_2O_3: (a) 0.0 mol%, (b) 0.05 mol%, (c) 0.1 mol%, and (d) 0.25 mol%.

scanning electron microscope (FESEM, Quanta 200, FEI, Brno, Czech). The average grain size (d) was determined by the lineal intercept method, given by the following expression $d=1.56\,L/MN$, where L is the random line length on the micrograph, M is the magnification of the micrograph, and N is the number of the grain boundaries intercepted by the lines [18]. The crystalline phases were identified by powder X-ray diffractometer (XRD, X′pert-PRO MPD, Panalytical, Almelo, Netherlands) with Ni filtered CuK_α radiation. The compositional analysis for minor phases was carried out by an energy dispersion X-ray spectroscope (EDS) attached to the SEM unit. The density of sintered pellet (ρ) was measured using a density determination kit (238490) attached to balance (AG 245, Mettler Toledo International Inc., Greifensee, Switzerland).

2.3. Electric filed–current density (E–J) measurement

The electric field (E)–current density (J) characteristics were measured using a high voltage source-measure unit (Keithley 237, Keithley Instruments Inc., Cleveland, OH, USA). The breakdown field (E_B) was measured at 1.0 mA/cm^2 and the leakage current density (J_L) was measured at 0.8 E_B. In addition, the nonlinear coefficient (α) is defined by the

Table 1
Microstructure, E–J, C–V, and dielectric parameters of the samples for different amounts of Er_2O_3.

Sample composition (all in mol%)	d (μm) ρ[a] (g/cm^3)	E_B (V/cm) v_{gb} (V/gb)	α J_L (μA/cm^2)	N_d (10^{17} cm^{-3}) Φ_b (eV)	N_t (10^{12} cm^{-2}) t (nm)	ε_{APP}' tanδ
$ZnO+0.5V_2O_5+2.0MnO_2+0.1Nb_2O_5$	4.4 5.52	6991 3.1	44 201	2.92 0.99	1.64 56.2	443.2 0.281
$ZnO+0.5V_2O_5+2.0MnO_2+0.1Nb_2O_5+0.05Er_2O_3$	4.3 5.56	7095 3.0	50 94	3.52 1.04	1.85 52.5	351.2 0.273
$ZnO+0.5V_2O_5+2.0MnO_2+0.1Nb_2O_5+0.1Er_2O_3$	4.2 5.57	7408 3.1	55 128	5.78 1.13	2.47 42.7	338.3 0.257
$ZnO+0.5V_2O_5+2.0MnO_2+0.1Nb_2O_5+0.25Er_2O_3$	4.6 5.59	6108 2.8	14 384	8.43 0.55	2.09 24.8	649.0 0.366

[a]Theoretical density 5.78 g/cm^3 for ZnO.

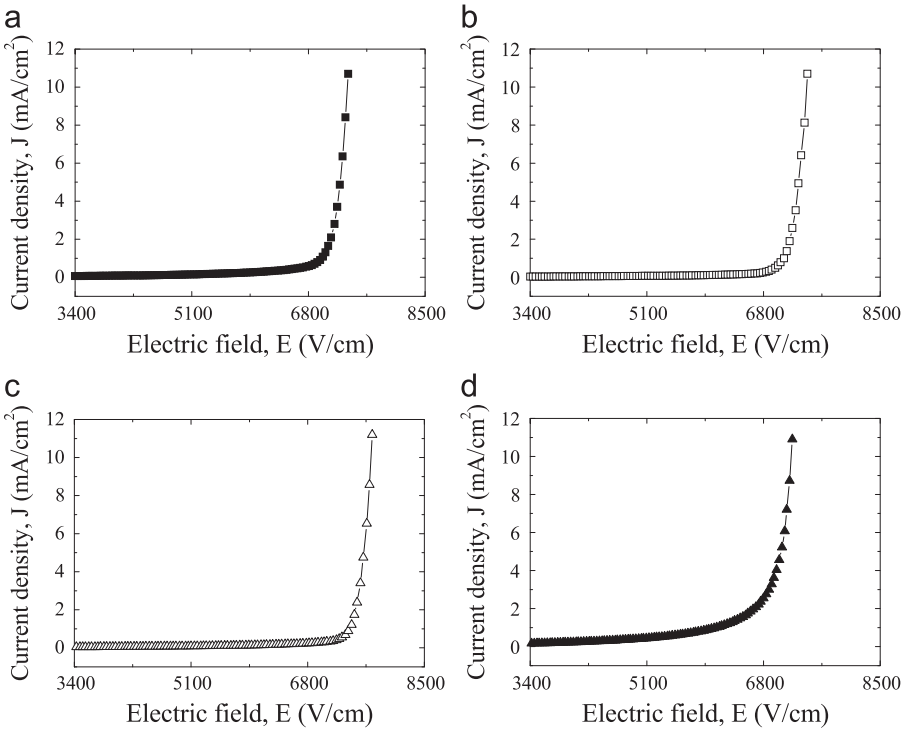

Fig. 3. E–J characteristics of the samples with different amounts of Er_2O_3: (a) 0.0 mol%, (b) 0.05 mol%, (c) 0.1 mol%, and (d) 0.25 mol%.

empirical law, $J=KE^{\alpha}$, where J is the current density, E is the applied electric field, and K is a constant. The α was determined by the following expression $\alpha=(\log J_2-\log J_1)/(\log E_2-\log E_1)$, where $J_1=1.0\ \mathrm{mA/cm^2}$ and $J_2=10\ \mathrm{mA/cm^2}$, E_1 and E_2 are the electric field corresponding to J_1 and J_2, respectively.

2.4. Capacitance–voltage (C–V) measurement

The capacitance (C)–voltage (V) characteristics were measured at 1 kHz and 1 V_{rms} using an RLC meter (QuadTech 7600, Marlborough, MA, USA) and an electrometer (Keithley 617, Keithley Instruments Inc., Cleveland, OH, USA). The donor concentration (N_d) of ZnO grains and the barrier height (Φ_b) at the grain boundary were determined by the following expression $(1/C_b-1/2C_{bo})^2=2(\Phi_b+V_{gb})/q\varepsilon N_d$ proposed by Mukae et al. [19], where C_b is the capacitance per unit area of a grain boundary, C_{bo} is the value of C_b when $V_{gb}=0$, V_{gb} is the applied voltage per grain boundary, q is the electronic charge, and ε is the permittivity of ZnO ($\varepsilon=8.5\varepsilon_o$). The density of interface states (N_t) at the grain boundary was determined by the following expression $N_t=(2\varepsilon N_d\Phi_b/q)^{1/2}$ [19] using the value of the donor concentration and barrier height obtained above. Once the donor concentration and barrier height are known, the depletion layer width (t) of the either side at the grain boundaries was determined by the following expression $N_d t=N_t$ [20].

2.5. Dielectric measurement

The dielectric behavior in accordance with frequency the apparent dielectric constant (ε_{APP}') and dissipation factor

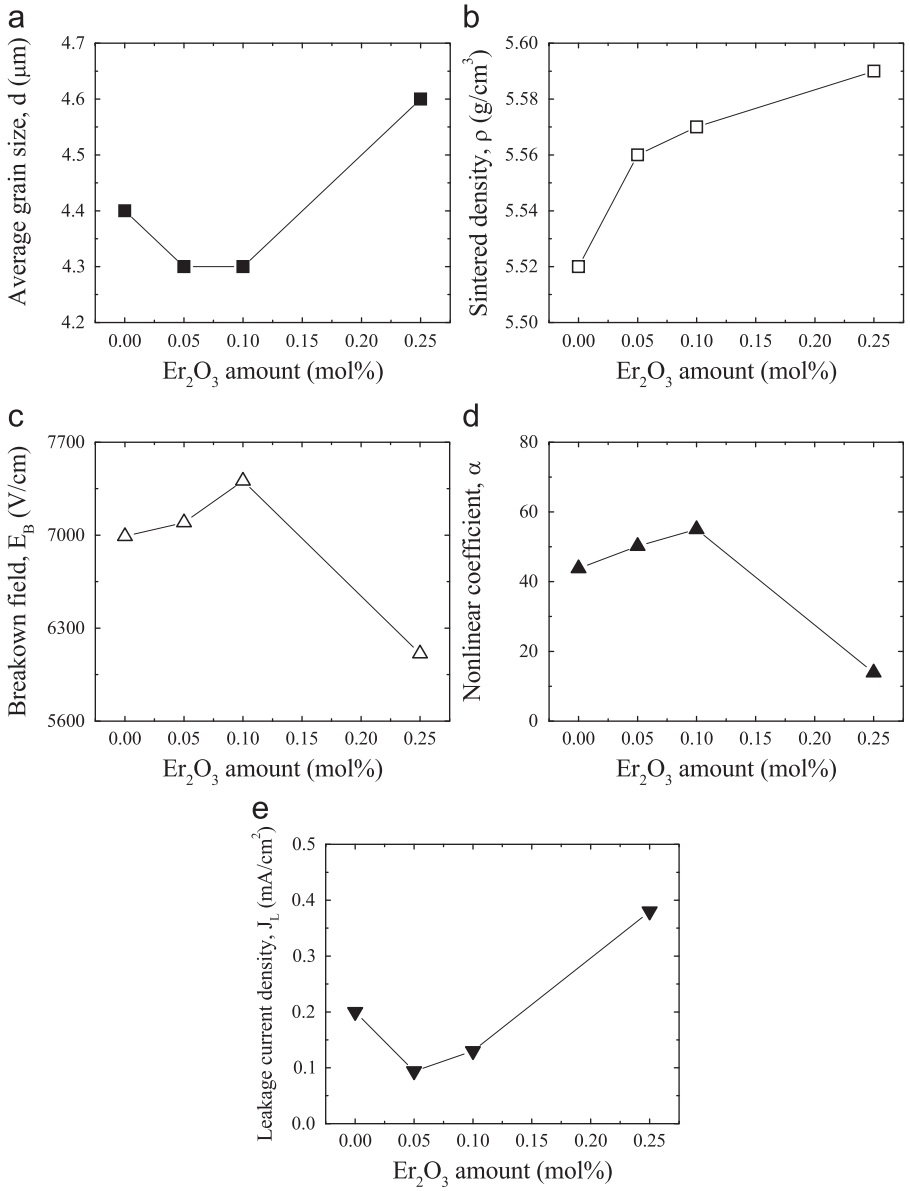

Fig. 4. E–J parameters as a function of Er_2O_3 amount of the samples: (a) average grain size, (b) sintered density, (c) breakdown field, (d) nonlinear coefficient, and (e) leakage current density.

(tanδ) of the samples were measured in the range of 100 Hz–2 MHz using a RLC meter (QuadTech 7600, Marlborough, MA, USA).

3. Results and discussion

Fig. 1 shows the SEM micrographs of the samples with different amounts of Er_2O_3. The average grain size decreased very slightly from 4.4 to 4.2 μm up to 0.1 mol% Er_2O_3 (see Fig. 4(a) in advance). Further addition increased it. The density of sintered pellet increased from 5.52 to 5.59 g/cm^3 corresponding to 95.5–96.7% of the theoretical density (TD) (pure ZnO, TD = 5.78 g/cm^3) (see Fig. 4(b) in advance). The XRD patterns in all the samples, as shown in Fig. 2, revealed the presence of $Zn_3(VO_4)_2$, ZnV_2O_4, $ErVO_4$, V_2O_5, and Mn-rich as a secondary phase, together with a primary phase of hexagonal ZnO. From EDS microanalysis (not shown in Fig), the *V* species was not found at the grain interior and Mn species was found at the grain interior and grain interiors [11]. Furthermore Mn species generated Mn-rich phase into ZnO grain and grain boundaries, and Mn-rich phase contains Nb species. The Mn and Nb species were also found at $Zn_3(VO_4)_2$ or ZnV_2O_4. The detailed microstructure parameters are summarized in Table 1.

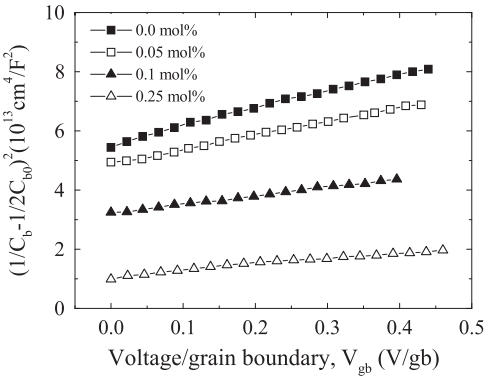

Fig. 5. *C–V* characteristics of the samples with different amounts of Er_2O_3.

Fig. 3 shows the *E–J* characteristics of the samples with different amounts of Er_2O_3. The varistor properties are characterized by non-linearity in the *E–J* curves. The samples added with 0.05 and 0.1 mol% Er_2O_3 were highly resistive, and a highly nonlinear electrical behavior was also found. However, the samples added with 0.25 mol% Er_2O_3 were less resistive compared with the Er_2O_3-free sample. The detailed *E–J* characteristic parameters are summarized in Table 1.

The behavior of breakdown field (E_B) as a function of Er_2O_3 amount was indicated graphically in Fig. 4(c). The breakdown field (E_B) significantly increased from 6991 to 7408 V/cm with an increase in the amount of Er_2O_3 up to 0.1 mol%. Then a further addition caused E_B to decrease,

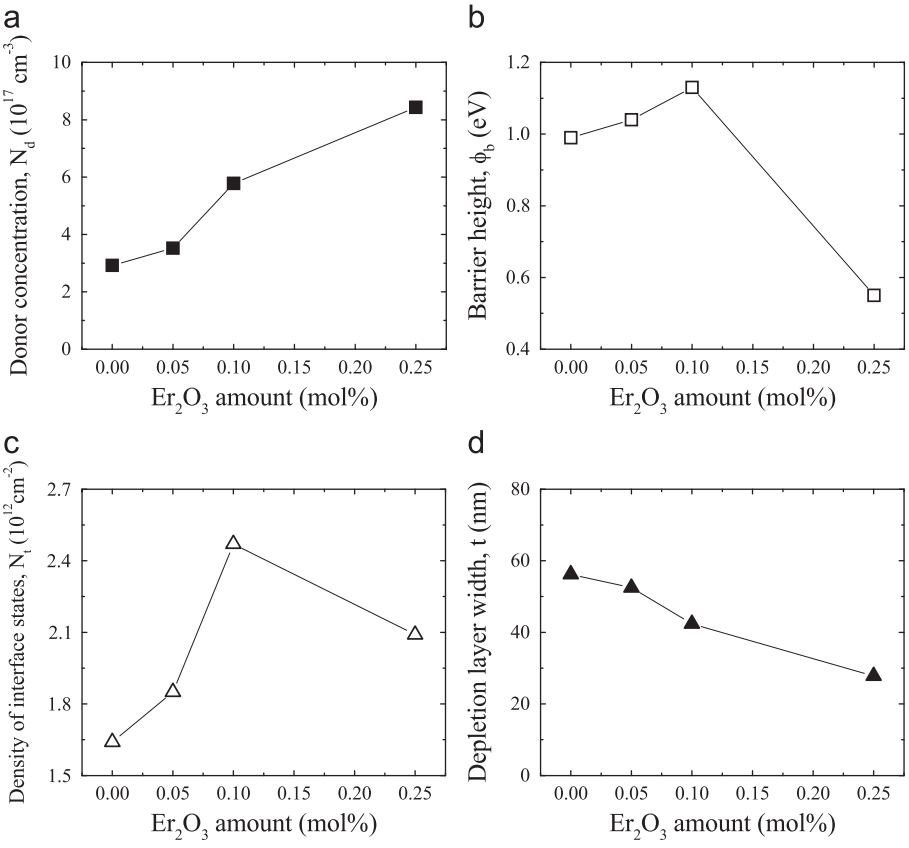

Fig. 6. *C–V* parameters as a function of Er_2O_3 amount: (a) donor concentration, (b) density of interface states, (c) barrier height, and (d) depletion layer width.

reaching 6108 V/cm at 0.25 mol% Er_2O_3. The behavior of E_B in accordance with the amount of Er_2O_3 can be explained by the average ZnO grain size. The increase of average grain size leads to the decrease of the number of grain boundary. This gives rise to the decrease of E_B. It is assumed that all the samples exhibited active grain boundaries, as showing the general value of 2–3 V/gb in the breakdown voltage per grain boundary.

The behavior of nonlinear coefficient (α) as a function of Er_2O_3 amount was indicated graphically in Fig. 4(d). The sample with no Er_2O_3 exhibited highly nonlinear properties, reaching 44 in nonlinear coefficient. Therefore, this composition is also new experimental result obtained in the study. Furthermore, the samples added with 0.1 mol% in the amount of Er_2O_3 exhibited the highest nonlinear properties, with a maximum value ($\alpha=55$). This is a surprising fact. It comes as a surprise to learn that the result appeared in the pellet sintered at 875 °C. Further addition caused α to decrease abruptly to 14 at 0.25 mol% Er_2O_3. When the amount of Er_2O_3 exceed 0.25 mol%, the abrupt decrease in the α value may be attributed to the lowering of the Schottky barrier. This is due to the abrupt variation of the electronic state at the grain boundary.

The behavior of leakage current density (J_L) as a function of Er_2O_3 amount was indicated graphically in Fig. 4(e). The behavior of leakage current density (J_L) in accordance with the amount of Er_2O_3 is inversely proportional to the α behavior. The J_L was the minimum value (94 μA/cm^2) at 0.05 mol% Er_2O_3. Further addition caused J_L to increase to 0.4 mA/cm^2 at 0.25 mol% Er_2O_3. On the whole, these composition proposed was found to exhibit high leakage current below expectations, compared with high nonlinear coefficient. In general ZnO–V_2O_5-based varistor ceramics exhibit a relatively high leakage current [10], compared with ZnO–Pr_6O_{11}-based varistors [3,4]. As a result, it was confirmed that the Er_2O_3 doping exhibits a strong effect on the nonlinear properties.

Fig. 5 shows the capacitance–voltage (C–V) characteristics of the samples with different amounts of Er_2O_3. The detailed C–V characteristic parameters, such as donor concentration (N_d), barrier height (Φ_b), density of interface states (N_t), and depletion layer width (t) are summarized in Table 1. The behavior of N_d as a function of Er_2O_3 amount was indicated graphically in Fig. 6(a). The N_d noticeably increased from 2.92×10^{17} to 8.43×10^{17} cm^{-3} with an increase in the amount of Er_2O_3. The Er^{3+} may be partially substituted in the Zn^{2+} site, because the Er^{3+} ionic radius (0.088 nm) is smaller than the Zn^{2+} ionic radius (0.074 nm). Where, the chemical-defect reaction using Kroger–Vink notation can be written as the following expression:

$$Er_2O_3 \xrightarrow{ZnO} 2Er^{\bullet}_{Zn} + 2O_O + 1/2O_2 + 2e'$$

Obviously, the Er^{3+} served as a donor-like because the addition of Er_2O_3 generates the electron in the conduction band based on the chemical-defect reaction. The behavior of Φ_b as a function of Er_2O_3 amount was indicated graphically in Fig. 6(b). The Φ_b at the grain boundaries increased in the range of 0.99–1.13 eV with an increase in the amount of Er_2O_3 up to 0.1 mol%. Further addition caused Φ_b to decrease to 0.55 eV at 0.25 mol%. The behavior of N_t as a function of Er_2O_3 amount was indicated graphically in Fig. 6(c). The N_t at the grain boundaries increased in the range of 1.64×10^{12} to 2.47×10^{12} cm^{-2} with an increase in the amount of Er_2O_3 up to 0.1 mol%. Further addition caused N_t to decrease to 2.09×10^{12} cm at 0.25 mol%. The behavior of t as a function of Er_2O_3 amount was indicated graphically in Fig. 6(d). The t value on either side of depletion region decreased in the range of 56.2 to 24.8 nm with an increase in the amount of Er_2O_3. This shows opposite relation to the N_d. In general, the depletion region extends farther into the side with a lighter doping.

Fig. 7 shows the dielectric characteristics of the samples for different amounts of Er_2O_3. As the frequency increased, the apparent dielectric constant (ε_{APP}') decreased, with first a

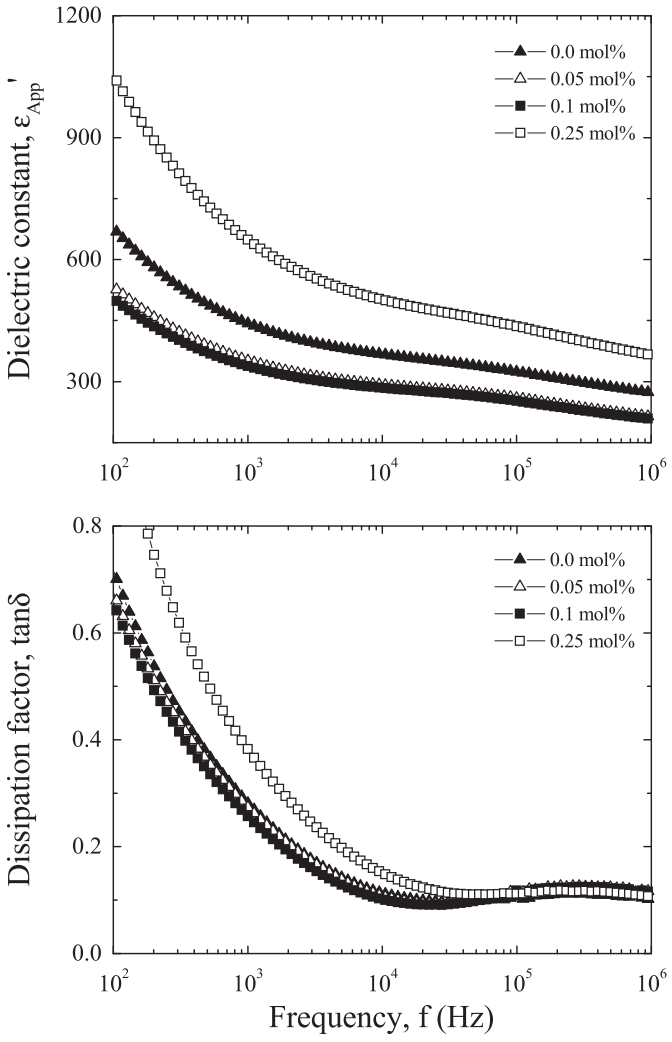

Fig. 7. Dielectric characteristics of the samples with different amounts of Er_2O_3.

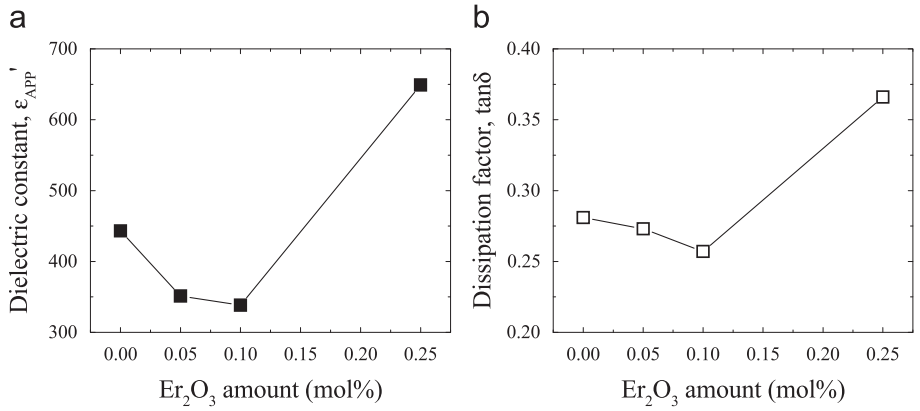

Fig. 8. Dielectric parameters as a function of Er_2O_3 amount: (a) apparent dielectric constant and (b) dielectric dissipation factor.

relatively sharp dispersive drop in the range of 100–1000 Hz and with second somewhat weak dispersive drop in the vicinity of 10^6 Hz. Considering polarization of dielectrics, This is attributed to the decrease of conduction carriers, which can follow to the test frequency. Experimental result for ε_{APP}' indicated that the ε_{APP}' decreased up to 0.1 mol% Er_2O_3 over frequency range, whereas a further addition caused ε_{APP}' to increase. Obviously, this is strongly connected with the average grain size, as indicated in the following equation, $\varepsilon_{APP}' = \varepsilon_g(d/t)$, where ε_g is the dielectric constant of ZnO (8.5), d is the average grain size, and t is the depletion layer width of the both sides at the grain boundaries. The decrease in the average grain size results in the decrease in the ε_{APP}'. The more detailed dielectric characteristic parameters are summarized in Table 1. The behavior of ε_{APP}' as a function of Er_2O_3 amount was indicated graphically in Fig. 8(a). The ε_{APP}' at 1 kHz decreased from 443.2 to 338.3 up to 0.1 mol% with an increase in the amount of Er_2O_3, whereas a further addition strongly increased ε_{APP}' to 649 at 0.25 mol%. It can be seen that he behavior of dielectric constant is similar to the behavior of breakdown field in the E–J characteristics, which strongly depend on average grain size. On the other hand, it can be seen that the dissipation factor (tanδ) decreased abruptly until the vicinity of 10 kHz with an increase of frequency for all samples, as indicated Fig. 7. A weak dielectric absorption peak exhibited in the vicinity of 200 kHz. The behavior of tanδ as a function of Er_2O_3 amount was indicated graphically in Fig. 8(b). The tanδ at 1 kHz value decreased from 0.281 to 0.257 up to 0.1 mol% with an increase in the amount of Er_2O_3, whereas a further addition increased tanδ to 0.366 at 0.25 mol%.

4. Conclusions

The ZnO–V_2O_5-based ceramics modified with erbium additives have been sintered at 875 °C, which is unusual low temperature in ceramics. The effect of Er_2O_3 incorporation on electrical properties was investigated. As the amount of Er_2O_3 increased, the density of sintered pellet increased, whereas the average grain size was found to have a fluctuation. The breakdown field increased up to 0.1 mol% with an increase in the amount of Er_2O_3, whereas a further addition decreased it. The nonlinear coefficient exhibited the same tendency as the breakdown field with an increase in the amount of Er_2O_3. Er_2O_3 acted as a donor due to the increase of the donor concentration with an increase in the amount of Er_2O_3. The apparent dielectric constant and the dielectric dissipation factor strongly depended on the average grain size and the leakage current density, respectively. Conclusively, considering nonlinear coefficient, the amount of Er_2O_3 was optimized at 0.1 mol%.

References

[1] L.M. Levinson, H.R. Philipp, Zinc oxide varistor-a review, American Ceramic Society Bulletin 65 (1986) 639–646.
[2] T.K. Gupta, Application of zinc oxide varistor, Journal of the American Ceramic Society 73 (1990) 1817–1840.
[3] C.W. Nahm, The nonlinear properties and stability of ZnO–Pr_6O_{11}–CoO–Cr_2O_3–Er_2O_3 ceramic varistors, Materials Letters 47 (2001) 182–187.
[4] C.W. Nahm, ZnO–Pr_6O_{11}–CoO–Cr_2O_3–Er_2O_3–based ceramic varistors with high stability of nonlinear properties, Journal of Materials Science Letters 21 (2002) 201–204.
[5] J.K. Tsai, T.B. Wu, Non-ohmic characteristics of ZnO–V_2O_5 ceramics, Journal of Applied Physics 76 (1994) 4817–4822.
[6] J.K. Tsai, T.B. Wu, Microstructure and nonohmic properties of binary ZnO–V_2O_5 ceramics sintered at 900 °C, Materials Letters 26 (1996) 199–203.
[7] C.T. Kuo, C.S. Chen, I.N. Lin, Microstructure and nonlinear properties of microwave-sintered ZnO–V_2O_5 varistors: I, effect of V_2O_5 doping, Journal of the American Ceramic Society 81 (1998) 2942–2948.
[8] H.H. Hng, K.M. Knowles, Characterization of $Zn_3(VO_4)_2$ phases in V_2O_5-doped ZnO varistors, Journal of the European Ceramic Society 19 (1999) 721–726.
[9] H.H. Hng, K.M. Knowles, Microstructure and current–voltage characteristics of multicomponent vanadium-doped zinc oxide varistors, Journal of the American Ceramic Society 83 (2000) 2455–2462.
[10] H.H. Hng, P.L Chan, Effects of MnO_2 doping in V_2O_5-doped ZnO varistor system, Materials Chemistry and Physics 75 (2002) 61–66.
[11] C.W. Nahm, Effect of MnO_2 addition on microstructure and electrical properties of ZnO–V_2O_5-based varistor ceramics, Ceramics International 35 (2009) 541–546.
[12] C.W. Nahm, Effect of sintering temperature on varistor properties and aging characteristics of ZnO–V_2O_5–MnO_2 ceramics, Ceramics International 35 (2009) 2679–2685.

[13] C.W. Nahm, Preparation and varistor properties of new quaternary Zn–V–Mn–(La, Dy) ceramics, Ceramics International 35 (2009) 3435–3440.
[14] C.W. Nahm, Influence of Nb addition on microstructure, electrical, dielectric properties, and aging behavior of MnCoDy modified Zn–V-based varistors, Journal of Materials Science: Materials in Electronics 21 (2010) 540–547.
[15] C.-W. Nahm, Effect of dopant (Al, Nb, Bi, La) on varistor properties of $ZnO–V_2O_5–MnO_2–Co_3O_4–Dy_2O_3$ ceramics, Ceramics International 36 (2010) 1109–1115.
[16] C.W. Nahm, DC accelerated aging behavior of Co–Dy–Nb doped Zn–V–M-based varistors with sintering process, Journal of Materials Science: Materials in Electronics 22 (2011) 444–451.
[17] C.W. Nahm, Er_2O_3 doping effect on electrical properties of $ZnO–V_2O_5–MnO_2–Nb_2O_5$ varistor ceramics, Journal of the American Ceramic Society 94 (2011) 3227–3229.
[18] J.C. Wurst, J.A. Nelson, Lineal intercept technique for measuring grain size in two-phase polycrystalline ceramics, Journal of the American Ceramic Society 55 (1972) 109–111.
[19] M. Mukae, K. Tsuda, I. Nagasawa, Capacitance-vs-voltage characteristics of ZnO varistor, Journal of Applied Physics 50 (1979) 4475–4476.
[20] L. Hozer, Semiconductor Ceramics: Grain Boundary Effects, Ellis Horwood, London, 1994, pp. 86–87.